Atmospheric Environment 45 (2011) 4481–4487

Contents lists available at ScienceDirect

Atmospheric Environment

journal homepage: www.elsevier.com/locate/atmosenv

A cellphone based system for large-scale monitoring of black carbon

N. Ramanathan [a,b,*], M. Lukac [b], T. Ahmed [c], A. Kar [d], P.S. Praveen [c,e], T. Honles [a], I. Leong [a], I.H. Rehman [d], J.J. Schauer [f], V. Ramanathan [c]

[a] Center for Embedded Networked Sensing, University of California, Los Angeles, 3563 Boelter Hall, Los Angeles, CA 90095-1596, USA
[b] Nexleaf Analytics, 2356 Pelham Ave., Los Angeles, CA 90064, USA
[c] Center for Clouds, Chemistry and Climate, Scripps Institution of Oceanography, University of California, San Diego, 9500 Gilman Drive, MC 0221, La Jolla, CA 92093-0221, USA
[d] The Energy and Resources Institute, Darbari Seth Block, IHC Complex, Lodhi Road, New Delhi 110003, India
[e] The United Nations Environment Programme, P.O. Box 30552, Nairobi, Kenya
[f] University of Wisconsin, 148 Water Science and Engineering Laboratory, 660 North Park Street, Madison, WI 53706-1484, USA

ARTICLE INFO

Article history:
Received 17 November 2010
Received in revised form
6 May 2011
Accepted 9 May 2011

Keywords:
Black carbon monitoring
Cellphone sensing
Soot sensor

ABSTRACT

Black carbon aerosols are a major component of soot and are also a major contributor to global and regional climate change. Reliable and cost-effective systems to measure near-surface black carbon (BC) mass concentrations (hereafter denoted as [BC]) globally are necessary to validate air pollution and climate models and to evaluate the effectiveness of BC mitigation actions. Toward this goal we describe a new wireless, low-cost, ultra low-power, BC cellphone based monitoring system (BC_CBM). BC_CBM integrates a Miniaturized Aerosol filter Sampler (MAS) with a cellphone for filter image collection, transmission and image analysis for determining [BC] in real time. The BC aerosols in the air accumulate on the MAS quartz filter, resulting in a coloration of the filter. A photograph of the filter is captured by the cellphone camera and transmitted by the cellphone to the analytics component of BC_CBM. The analytics component compares the image with a calibrated reference scale (also included in the photograph) to estimate [BC]. We demonstrate with field data collected from vastly differing environments, ranging from southern California to rural regions in the Indo-Gangetic plains of Northern India, that the total BC deposited on the filter is directly and uniquely related to the reflectance of the filter in the red wavelength, irrespective of its source or how the particles were deposited. [BC] varied from 0.1 to 1 $\mu g\,m^{-3}$ in Southern California and from 10 to 200 $\mu g\,m^{-3}$ in rural India in our field studies. In spite of the 3 orders of magnitude variation in [BC], the BC_CBM system was able to determine the [BC] well within the experimental error of two independent reference instruments for both indoor air and outdoor ambient air.

Accurate, global-scale measurements of [BC] in urban and remote rural locations, enabled by the wireless, low-cost, ultra low-power operation of BC_CBM, will make it possible to better capture the large spatial and temporal variations in [BC], informing climate science, health, and policy.

Published by Elsevier Ltd.

1. Introduction

Black carbon (BC), the strongly light-absorbing component of soot that gives emissions such as diesel engine exhaust and smoke plumes their dark, brownish color, has come to be recognized as a major contributor to global warming (Ramanathan and Carmichael, 2008; Jacobson, 2010). BC has now become a frontline concern for climate change strategies (Jacobson, 2010; Ramanathan and Xu, 2010). Generated from the incomplete combustion of fossil fuel, and the burning of biomass fuels, such as wood, dung and crop residues (Bond et al., 2007; Venkataraman et al., 2010), BC is the dominant aerosol component absorbing solar radiation in the air which has significant regional and global climate impacts, particularly in the tropical and arctic regions (Ramanathan and Carmichael, 2008; Shindell and Faluvegi, 2009; Flanner et al., 2009). In addition to BC's climate impacts, the inhalation of smoke containing BC results in more than 1.8 million deaths per year (Ezzati and Kamen, 2002; Pachauri and Sridharan, 1998).

BC also represents something of an opportunity for climate mitigation initiatives. Unlike CO_2, which can remain in the air for centuries, the atmospheric lifespan of BC is of the order of weeks or even days (IPCC, 2007). The opportunity then derives from the fact that almost any mitigation actions (even at local scales) of BC

* Corresponding author. Center for Embedded Networked Sensing, University of California, Los Angeles, 3563 Boelter Hall, Los Angeles, CA 90095-1596, USA.
E-mail address: nithya@cs.ucla.edu (N. Ramanathan).

1352-2310/$ – see front matter Published by Elsevier Ltd.
doi:10.1016/j.atmosenv.2011.05.030

emissions should have a swift and tangible impact on climate change and health. Given the factor of 2 or more uncertainties in BC emission inventories (IPCC, 2007), the localized nature of BC emissions (from individual trucks, indoor cooking, brick kilns, etc.) and the short life times, we need a cost-effective, accurate and scalable measurement system for determining near-surface [BC] for verifying and validating the effectiveness of BC mitigation actions. Such high resolution spatial and temporal BC data are also needed for climate and health impact studies. We have developed such a system, described in Section 2 and evaluated in Section 3.

1.1. The principal features and merits of the BC_CBM system

The BC_CBM system consists of three sub-systems: i) The Miniaturized Aerosol filter Sampler (MAS). ii) The cellphone to capture the image of the exposed BC filter in the MAS. iii) The automated software algorithm for converting the reflectance in the "red" wavelength of the exposed MAS BC filter to its corresponding [BC] in real time. We use reflectance in the red spectrum, which corresponds to wavelengths of approximately 630–740 nm.

Our new system is designed to facilitate large-scale [BC] measurements in a low-power, cost-efficient manner without compromising the quality of the data (Ramanathan et al., 2010). Leveraging the resolution, capacity, noise level and dynamic range of conventional cellphone cameras, the MAS and analytic process utilizes photographs of the BC deposited on air filters in order to derive [BC]. Taking advantage of that efficiency, our system enhances the process of BC data collection by enabling measurements in locations where data had been previously difficult to secure in a predictable and standardized format due to the prohibitive cost and the logistical complexity of implementing monitoring tools.

There are two prevailing filter-based methods for collecting [BC] data on a large scale: optically based real-time BC monitoring methods (such as the Aethalometer from Magee Scientific) which utilize light-absorbing characteristic of BC aerosols for measurement (Hansen et al., 1984); and thermal-optical methods (destructive thermal evolution techniques) which utilize thermal and chemical refractory properties for measurement of BC samples collected over a period of several hours (Chow et al., 1993; Birch and Carry, 1996). We use the National Institute for Occupational Safety and Health (NIOSH) thermal-optical transmittance protocol (TOT) for the thermal-optical method (NIOSH, 1996). For a comparison of NIOSH and IMPROVE protocols see Chow et al. (2001).

Both these BC measurement techniques pose a challenge in terms of their high upfront cost and level of technical expertise required for operation. Thermal-optical analyses require preservation and shipping of the filters after collection to a central laboratory where the analyses are done at a cost of approximately $50 per filter. Daily measurements for a year using this approach would cost approximately $18,250. Operation for one year of an Aethalometer would cost approximately $21,000, and of a micro-Aethalometer would cost approximately $7300. Other instruments are more expensive. In comparison, deployment and collection of daily samples for one year using BC_CBM would cost less than $1000, and measurements would be available in real time.

It is important to note that BC_CBM is not meant to be a substitute for more sophisticated measurements which need to be done. More than 40% of global BC emissions come from biomass burning, to which Africa and Asia are major contributors (Bond et al., 2007). It is in such rural or resource-constrained locations where a light-weight, affordable, measurement system like BC_CBM would complement more sophisticated measurement methods (e.g. Aethalometer, thermal-optical methods, Particle soot absorption photometer, Photoacoustic spectrometer or Single particle soot photometer (Bond et al., 1999; Arnott et al., 1999; Stephens et al., 2003; Schwarz et al., 2006)), and revolutionize our understanding of BC through increased spatial measurements.

1.2. Deployment with Project Surya

BC_CBM was developed to compare clean cook stove technologies against traditional mud stove based meal preparation methods in the context of Project Surya (Ramanathan and Balakrishnan, 2007; www.projectsurya.org). Project Surya will replace the highly polluting cooking methods traditionally employed in rural areas with clean cookstoves and document the climate and the health impacts. BC_CBM was deployed as part of Project Surya to collect data on outdoor [BC], and indoor [BC] and individual exposure on a household level from February to June 2010.

2. Experimental description of BC_CBM

2.1. Miniaturized Aerosol filter Sampler (MAS)

Fig. 1a shows our Miniaturized Aerosol filter Sampler (MAS) system for BC measurement. MAS houses four main components in a plastic enclosure measuring 160 mm × 160 mm × 89 mm: (i) a battery operated micro air pump (manufactured by Sensidyne Inc., AAA series micro air pump model-20) (ii) a 25-mm diameter closed aluminum filter holder (BGI Inc., Waltham, MA) (iii) a battery for continuous power supply and (iv) control electronics. The micro pump (which measures approximately 41 mm × 17 mm × 28 mm) draws air through a 25-mm diameter quartz filter placed inside the filter holder, and can operate at a maximum flow rate of 625 cc min^{-1}.

The MAS system requires approximately 336 mW of power, consuming substantially less power than any commercially available single-wavelength or multi-wavelength BC measuring instrument. The MAS' rechargeable Li-Ion battery (14.8 V, 2200 mAh) is capable of running the micro air pump continuously for up to 100 h. A digital flow meter is included with feedback loop to monitor and log flow rate as constant flow rate is critical for measurement reliability. The control electronics have a DC–DC converter to provide a steady 12-V supply, and can control the pump flow rate (e.g., to reduce the flow rate in highly polluted regions), and the sampling schedule (e.g., in order to save power, the sampler can be turned on for shorter periods throughout the day). The controller utilizes a real-time 24-h clock operated off of an independent coin-battery power source. In addition to battery power, the MAS system can also run off of AC power using an AC-to-DC adapter.

The loading of particles on the filter is captured by measuring the reflectance from the filter in the red wavelength (represented by the symbol ρ_{red}). This can be done using a photoelectric meter or a standard scanner. Through laboratory and field testing of this idea by us and others (Cheng et al., 2011), it has been shown that ρ_{red} for a filter is strongly related to the total loading of BC that accumulates on that filter (measured in BC mass per unit area on the filter, using units of [$\mu g\ cm^{-2}$]) (Ramanathan et al., 2010). In fact, the approach of linking filter color with particulate pollution has a long history (see the review in Moosmüller et al., 2009).

The primary insight resulting from our work is that ρ_{red} is a reliable indicator of absorption by BC, and can be measured from an image of a filter that is captured with a cellphone camera, with accuracy to within 20% of a BC reference instrument. We use the RGB (red, green, blue) color space to describe the reflectance of the BC particles from the image of the filter. We measure ρ_{red} by extracting the red chromaticity of the filter from the cellphone image. The results of our tests show that this estimate of ρ_{red} for the BC accumulated on the filter can be used to accurately estimate the total loading of BC accumulated on the filter. Given the image of

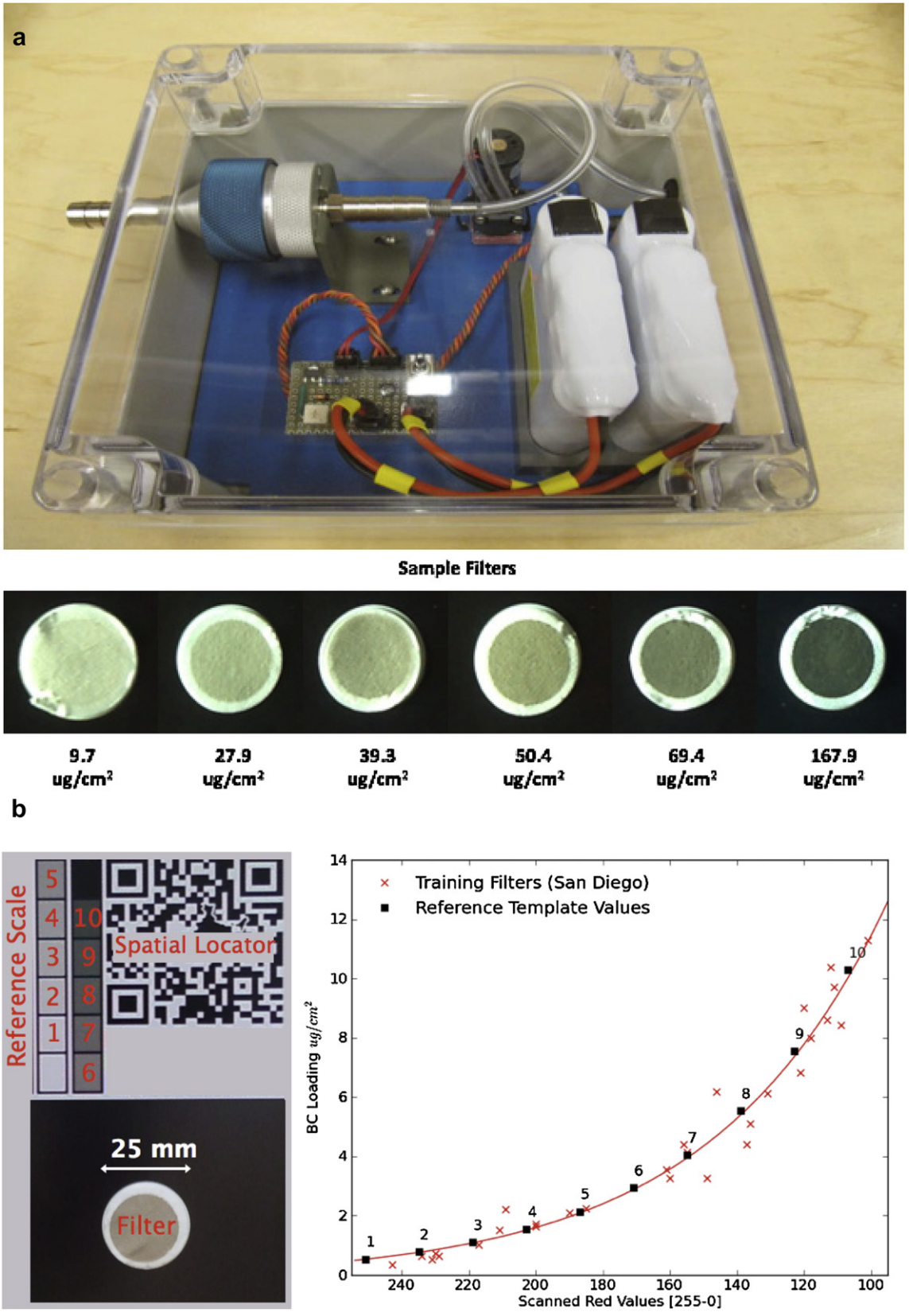

Fig. 1. (a). (top) Photograph of Miniaturized Aerosol filter Sampler (MAS) system. MAS houses four main components in a plastic enclosure (i) a battery operated micro air pump, (ii) a 25-mm closed aluminum filter holder, (iii) a battery for continuous power supply, and (iv) control electronics. (bottom) A series of sample filters shown which vary from light to dark, and from low to high BC loading (BC_l) respectively. (b). (left) The labeled image of the template (containing the spatial locator and reference scale) and filter as seen by the computer algorithm (without the labels). The reference scale is created using the colors that correspond to the 10 points on the calibration curve. (right) Calibration curve showing the best exponential fit-line for color (obtained from a scanned image) to BC loading (BC_l) accumulated on the filter. The reference scale colors and corresponding BC_l are marked as black squares on the calibration curve.

the filter and the total volume of air that has passed through the filter, the [BC] can be calculated.

2.2. Algorithm to convert ρ_{red} for the exposed MAS BC filter to [BC]

The procedure to determine [BC] using MAS involves the following steps:

i) Collect Training Dataset: Collect training filter samples of BC using the MAS system. Loading on the filter should be varied either by varying the exposure duration or [BC]. Determine the BC loading corresponding to each training filter using a reference instrument. Scan each filter in using an image scanner to determine ρ_{red} of the BC particles accumulated on the filter.

ii) Create Reference Scale: Create the calibration curve using the training dataset to map ρ_{red} to BC loading (shown in Fig. 1b). Identify 10 points along this curve (i.e. low BC loading to high BC loading in 10 steps). Using the ρ_{red} that corresponds to each of the 10 points in the training calibration curve, print the 10 shades in the reference scale. The scale varies from light to dark gray, and each shade in the reference scale corresponds to a different BC loading value. The entire template (including the reference scale) is shown in Fig. 1b.

iii) Analyze New Sample: Place the filter on the template, and take a photograph (sample photograph shown in Fig. 1b). The algorithm automatically reconstructs the calibration curve for this image by extracting ρ_{red} for each shade in the reference scale, and matching each value with the known BC loading associated with that shade. The ρ_{red} of the filter is then extracted, and plugged into this new calibration curve to obtain the BC loading on the filter. The algorithm automatically determines [BC] using the flow rate of the pump, the sampling duration, and the area of the BC particles collected on the filter.

Steps (i) and (ii) are required for calibration, and only need to be done once: Remarkably, our results show that the same reference scale could be used to analyze samples collected in California and in India. Step (iii) is the only step required to collect [BC] measurements. These steps are further described in Sections 2.2.1–2.2.3.

2.2.1. Collection and determination of BC loading on training filters

41 BC filters were collected in San Diego, California between June 2009 and February 2010 using the first MAS system (which relied on a vacuum pump instead of a low-power pump). A random subset of 29 of these filters was selected for the training dataset for the BC_CBM calibration curve. In order to calculate the BC loading associated with each training filter, the 7-wavelength Aethalometer (model AE-31) was deployed side by side with the MAS system, and BC aerosols were collected through the common aerosol inlet. Aethalometer data were used to calculate the BC loading (BC_l) for each filter using the following equation:

$$BC_l\ [\mu g/cm^2] = \frac{[BC]_{Aethalometer}\ [\mu g/m^3] \times V_f\ [m^3]}{A\ [cm^2]} \quad (1)$$

A [cm^2] is the area of the spot occupied by the BC particles deposited on the MAS filter, and is constant across filters; for our system A = 2.4 cm^2. V_f [m^3] is the volume of air that passes through the filter in the MAS, and can be different for each sample; it is the product of the MAS pump's mean flow rate, F [$m^3\ min^{-1}$], and the duration the filter was exposed in the MAS system, D [min], which varies and must be measured for each filter: $V_f = F\ [m^3\ min^{-1}] \times D$ [min]. F is measured before the instrument is deployed, and is also logged by the MAS sub-system as constant flow rate is critical for measurement reliability.

$[BC]_{Aethalometer}$ is the [BC] reported by the AE-31 at 880 nm. We follow the standard practice of using transmission data captured at 880 nm for determining [BC] because absorption of radiation of other aerosols (e.g. organic aerosols) are negligible at 880 nm (Kirchstetter et al., 2004; Chen and Bond, 2010).

2.2.2. Creating the reference scale

Creation of the reference scale requires the closest approximation possible to the actual ρ_{red} of the BC particles on a set of training filters. The training filters were scanned using a commercially available flatbed color digital scanner (Epson Perfection 4490 Photo scanner). ρ_{red} was manually extracted from the scanned image of the training BC filters using the GNU Image Manipulation Program (Gimp), a photo-editing tool. A calibration function, f, was derived to relate ρ_{red} values from each filter to the corresponding BC_l (Fig. 1b). Created with the training data collected in San Diego, empirically we found that the relationship between ρ_{red} and BC_l is exponential. The exponential fit-line has an r^2 of 0.97, and is represented with the equation:

$$BC_l\ [\mu g/cm^2] = f_{sf}(\rho_{red}) = -0.715 + 172.6045 \times e^{-0.0183 \times \rho_{red}} \quad (2)$$

Ten evenly spaced points were selected along this calibration curve (marked as black squares in the plot in Fig. 1b). The corresponding ρ_{red} for each point was used to create the 10 shades in the reference scale. When creating the reference scale, we used scanned images of the filters – instead of, for example, images of the filters taken with a camera – in order to minimize any inconsistencies across images that could be introduced by differing lighting and exposure. A scanner, however, presents several variables that can also introduce error, including variations in exposure and gamma. Nevertheless, by printing the reference scale, our goal was to create an image where each shade represents as closely as possible the reflectance of the filter corresponding to the given BC_l value.

In order to minimize error introduced by different inks, papers, and printing processes, the reference scale was printed using a recently profiled Noritsu QSS-3411 digital printer so as to match the RGB values extracted from the scanned images with the CMYK color space as accurately as possible. The reference scale is printed along with a spatial locator (described in Section 2.2.3). This template is shown in Fig. 1b. The entire template was printed with the matte finish to minimize glare that could arise when taking an image of the filter with a cellphone.

2.2.3. Determination of [BC] of actual sample

An exposed filter is removed from the MAS filter holder and placed on the template as shown in Fig. 1b. A cellphone is used to capture a photograph of the filter and the template and to transmit the image (by SMS, email or upload) to the BC_CBM server for analysis. The server automatically and almost immediately analyzes the image, and returns the corresponding [BC] value to the phone via SMS.

The algorithm scans the image, then rotates, stretches, and transforms the image until the spatial locator (labeled in Fig. 1b) is identified. The spatial locator is a QR code, which is a standard, fixed-size, two-dimensional bar code that the system uses to calibrate the size and position of all other elements on the image. The system uses the spatial locator as a landmark to find the reference scale (labeled in Fig. 1b). The system uses these two landmarks to crop the image, and reduce the search space required to find the filter. Running a circle detection method (called from the openCV

image analysis library), the system identifies the set of pixels that it deems to most likely be the filter, based on the size and shape.

The system then extracts ρ_{red} for the filter, and ρ_{red} for each shade in the reference scale. A set of pixels is sampled and averaged from each location in the image to minimize error. The 10-point dataset of ρ_{red} and the corresponding known BC_l for each shade in the reference scale is used to derive the function, f, which is used to calculate the BC loading on the exposed filter given ρ_{red} for the filter.

Both the filter and the reference scale are included in each image so that the function, f, can be derived for each cellphone image. This is done because one of the biggest variables influencing the measurement of color is the particular camera used for acquiring the filter; especially as modern digital imaging devices use sophisticated proprietary algorithms for color correction. The algorithm is built on the assumption that any ambient condition that will impact the calculation of ρ_{red} for the filter will, in general, uniformly impact the calculation of ρ_{red} for the reference scale as well. The reference scale therefore permits the calculation of ρ_{red} to be calibrated for different ambient conditions (such as light levels, camera angles, aerosol composition), cameras, and camera configurations. Furthermore, because the reference scale is present in each image, BC_CBM does not depend on blank analysis for each sample.

3. Results

3.1. Field deployments

BC_CBM has been deployed in two locations in southern California, San Diego (32°43′N, 117°10′W) and Los Angeles (34°3′N, 118°15′W), and in the rural village (26°28′N, 81°39′E) with a population of approximately 1300, located in the densely populated Indo-Gangetic Plains region of northern India. The MAS system was first deployed in various outdoor locations in San Diego, where 41 samples were collected from June 2009 to March 2010. (2 were rejected because the exposure duration for the sample was incorrectly recorded.) Of these, a random subset of 29 samples was used as a training dataset to calibrate the BC loading associated with each shade in the reference scale (Fig. 1b), and the remaining 8 samples were used for cross validation. After using the training data to create the calibration chart, the BC_CBM system was deployed in various locations around Los Angeles between June 18–25, 2010, including in one location within 2 miles of the Los Angeles International Airport. In all California locations, the samples were validated by comparing results from the MAS system with Aethalometer data to evaluate the accuracy in BC loading and [BC]. The raw Aethalometer data were corrected for filter loading and scattering artifacts using the method outlined in Schmid et al. (2006). The accuracy of the [BC] measurements reported by the Aethalometer is not well understood, and could be on the order of 50%, particularly when [BC] are low ($<0.1\ \mu g\ m^{-3}$).

There are two points we wish to make in this regard. In this study we have compared the [BC] determined by two independent reference methods to determine the uncertainty in the BC measurement. Further, the uncertainty in the BC_CBM is not limited by the uncertainty of the reference instruments. The training filters could also be calibrated with other BC measurement methods, for example with results from thermal-optical analysis of the filters using the NIOSH protocol, as evidenced by the close agreement between BC_CBM and NIOSH results seen in Fig. 2, for increased accuracy.

BC_CBM was deployed in India, where 67 BC filters were collected from February to June 2010 inside the rural kitchen (39 samples) as well as outdoor (28 samples) near the village center. All of the 67 India samples were exposed for approximately 24 h with the pump flow rate set at 570 cc min^{-1}. Cellphone images of all of the filters were taken by trained personnel and researchers. Results from these three field deployments are discussed in Section 3.2.

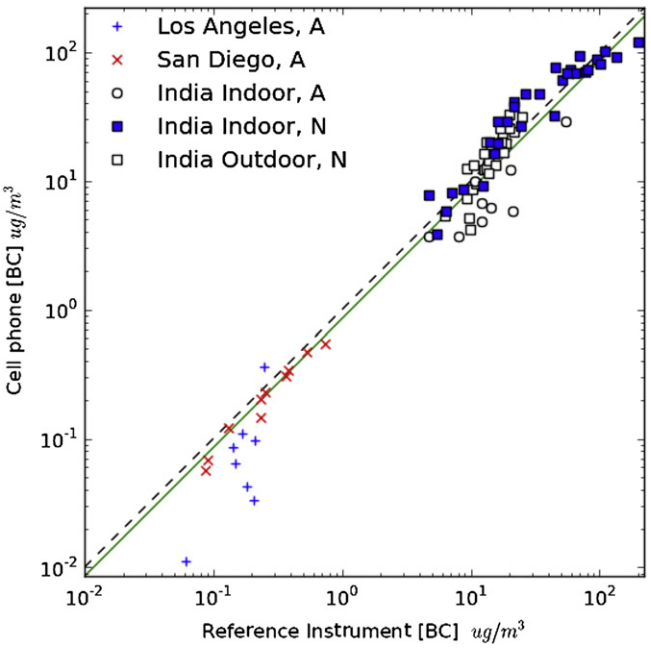

Fig. 2. [BC] reported by BC_CBM versus [BC] reported by the reference instrument for filters collected in San Diego, Los Angeles, and Khairatpur during 2009 and 2010. (Legend specifies which reference instrument used: a specifies an Aethalometer, and [BC] is reported; N specifies the data collected with a TOT method, and [EC] is reported.) Linear regression line in log–log space slope = 0.85, and $r^2 = 0.83$. RMS error for measurements less than or equal to 1 $\mu g\ m^{-3}$ is 0.02 $\mu g\ m^{-3}$, which is 8.5% of the mean; RMS error for measurements greater than 1 $\mu g\ m^{-3}$ is 1.8 $\mu g\ m^{-3}$, which is 6.0% of the mean.

For [BC] and [OC] determination from samples collected in India, samples were analyzed both with the Aethalometer and the NIOSH TOT protocol (Schauer et al., 2003). The data collected with the TOT method are referred to as EC (for elemental carbon), and the Aethalometer data are referred to as BC. The definitions of EC and BC are itself a bit arbitrary (see detailed discussions of this topic in Andreae and Gelencser, 2006). The definition of BC is an optical definition and includes contribution by some organic aerosols, whereas, EC measures are derived by thermal and chemical analyses and would tend to determine graphitic-like elemental carbon. During inter-comparisons of BC results from the two reference systems using samples collected in India, the systems agreed within 20%. [BC] collected with BC_CBM was compared with measurements from both methods to evaluate the accuracy of the BC_CBM system.

Four different cellphones were used to collect data: Nokia N80, Samsung SCH-S379, Samsung SCH-U490, and LG VX8300. Preliminary analysis demonstrates that measurements differ within our margin of error for BC_CBM analysis of images from different cellphones. This calibration across cellphones, each with cameras and software which employ their own proprietary algorithms for color correction and configuration, is accomplished using the reference scale.

3.2. Results

The calibration curve for the BC_CBM analytic sub-system was obtained from the San Diego training data, and this curve was used without any change when analyzing samples from California and India. BC_CBM data were obtained for 18 samples collected in Los Angeles and San Diego (not included in the training dataset), and 67

samples collected in India (both indoors and outdoors). Fig. 2 compares BC_CBM [BC] data with the reference system [BC] data in log–log space. Plots showing the same data, separately for California and India samples on a linear plot are listed in the Supporting Information (Supplement data). Three major characteristics of the comparison, shown in Fig. 2 and described below, demonstrate the validity of the BC_CBM system for global monitoring of BC:

i) In spite of the nearly 3 orders of magnitude variation in [BC] from 0.1 $\mu g\,m^{-3}$ to over 100 $\mu g\,m^{-3}$, the cellphone based [BC] agrees with the reference system [BC] with a root mean squared (RMS) error of less than 10%: RMS error for measurements less than or equal to 1 $\mu g\,m^{-3}$ is 0.02 $\mu g\,m^{-3}$, which is 8.5% of the mean; RMS error for measurements greater than 1 $\mu g\,m^{-3}$ is 1.8 $\mu g\,m^{-3}$, which is 6.0% of the mean measurement.
ii) The RMS error in the cellphone based measurements is similar across all of the 3 sampling locations. This is significant because the BC aerosols in the California sampling locations are primarily sourced by burning of fossil fuel, while the BC aerosols in the Indian sampling location is dominated by biomass-fuel cooking.
iii) The fact that RMS error is independent of the [BC] levels, regional location and the source of BC is remarkable because the same calibration curve was used to reduce the cellphone filter photographs to [BC] for all of the data sets.

These major characteristics inferred from Fig. 2 imply that the BC filter's reflectance in the red wavelength is uniquely related to the quantity of BC deposited on the filter, irrespective of its source or how these particles were deposited. We make this inference based on the following: First, sources which emit BC also co-emit OC aerosols. Some of these OC aerosols, referred to as brown carbon (Andreae and Gelencser, 2006), also absorb solar radiation. Absorption of solar radiation by brown carbon is particularly strong in the ultraviolet regions; absorption in the near infrared region (greater than 800 nm) is negligible; and absorption in the red region (620–750 nm) is less than 5% of the absorption in the ultraviolet regions (<400 nm) (Kirchstetter et al., 2004; Chen and Bond, 2010). Therefore, the interference of OC aerosol absorption on BC_CBM measurement of [BC] (which infers absorption in the red region, corresponding approximately to 630–740 nm) should be small or within the instrument's uncertainty. This assertion is confirmed in Fig. 3, which compares the Aethalometer [BC] at 880 nm, where brown carbon absorption is negligible, with the Aethalometer [BC] at 660 nm. (As mentioned earlier, we calibrate BC_CBM with the Aethalometer [BC] inferred from the 880 nm absorption.) The two [BC] values agree within 5%. This close agreement indicates that the impact of brown carbon absorption in the red region, which is used by BC_CBM, is within the experimental error (20%).

Next, there is close agreement between [BC] reported by BC_CBM and [BC] measurements from the two reference methods (one of which is a chemical method, and one of which is an optical method), even when analyzing data from two settings which contain different types of OC aerosols (Fig. 2). We measured [BC] concentrations in rural India, where aerosols are sourced primarily from biomass burning; and we measured [BC] concentrations in urban areas in California, where aerosols are sourced from fossil fuel and will have a lower proportion of [OC] compared to aerosols sourced from biomass (Bond et al., 2007) (because biomass burning emits significantly more OC).

Lastly, we consider it remarkable that the filter's reflectance in the red wavelength of the BC deposited on the filter, as captured by a cellphone, is uniquely related to the quantity of BC deposited on the filter. This is noteworthy especially because [BC] measurements by the BC_CBM are based on the reflection of radiation from the filter, while [BC] measurements by an Aethalometer are based on the transmission of radiation through the filter. Chen et al. (2004) provide a theoretical and experimental analysis on the relationship between transmission and reflection based measurements of BC.

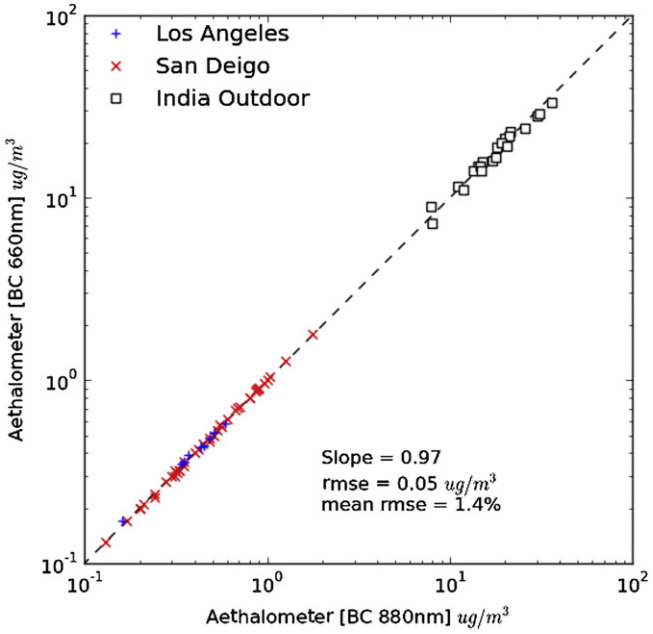

Fig. 3. Compares the Aethalometer [BC] at 880 nm where brown carbon absorption is negligible, with that at 660 nm. The two [BC] values agree within 5%.

4. Conclusions and implications

The principal finding of this study is that digital images of air filters that have been exposed to BC – including images that are created by widely available cellphone cameras – can be used to affordably and accurately estimate BC loading in real time, and can be applied toward determinations of BC emissions.

The [BC] shown in Figs. 2 and 3 have significant implications for climate and health, highlighting the need for rapid improvement in spatial measurements of BC. In southern California [BC] range from less than 0.1 $\mu g\,m^{-3}$ to 1 $\mu g\,m^{-3}$ which suggests that in spite of stringent emission controls, [BC] is still high with respect to regional climate and health standards. These high California concentrations are further dwarfed by the 1–25 $\mu g\,m^{-3}$ [BC] measured in outdoor air in India using BC_CBM. Such high concentrations have significant implications for the impact of aerosols on monsoon rainfall and on the Himalayan glacier retreat. The even larger [BC] in the range of 10–200 $\mu g\,m^{-3}$ measured indoors in India pose a grave threat to women and children subject to this soot laden smoke. The order of magnitude difference between outdoor and indoor measurements in India further show that outdoor measurements cannot be used as a proxy for indoor measurements.

The use of cellphones permits monitoring of BC to occur on a greater, comprehensive scale because of the ubiquity of cellphones and the wireless networks that they rely on. By taking advantage of existing, widespread wireless technologies and cellphone handsets, our BC measurement system creates a real time, ultra low-power, affordable, data-gathering mechanism from commonplace technical components that features a readily familiar interface. That familiarity has proven to help non-expert researchers from outside of the scientific community perform BC monitoring in remote and

resource-constrained locations (e.g. rural areas) where power is not readily available, broadening the geographic scope of the data-gathering process. It is likely that a similar approach can be used to collect climate, air pollution and human behavioral data. It is our hope that the findings of this study will unleash such developments.

Acknowledgments

The authors wish to acknowledge the Swedish International Development Agency, National Science Foundation (grant #AGS-1016496), United Nations Environment Programme, and Qualcomm Inc for funding and support. We thank Dr. E. Frieman for initiating this research, and Drs. M. Ramana and C. Corrigan for helping with the earlier stage of development.

Appendix. Supplementary data

Supplementary data associated with this article can be found, in the online version, at doi:10.1016/j.atmosenv.2011.05.030.

References

Andreae, M.O., Gelencser, A., 2006. Black carbon or brown carbon? The nature of light-absorbing carbonaceous aerosols. Atmospheric Chemistry and Physics 6, 3131–3148.

Arnott, W.P., Moosmüller, H., Rogers, C.F., Jin, T., Bruch, R., 1999. Photoacoustic spectrometer for measuring light absorption by aerosol: instrument description. Atmospheric Environment 33, 2845–2852.

Birch, M.E., Carry, R.A., 1996. Elemental carbon based for monitoring occupational exposures to particulate diesel exhaust. Aerosol Science and Technology 25, 221–241.

Bond, T.C., Anderson, T.L., Campbell, D., 1999. Calibration and intercomparison of filter-based measurements of visible light absorption by aerosols. Aerosol Science and Technology 30, 582–600.

Bond, T.C., Bhardwaj, E., Dong, R., Jogani, R., Jung, S., Roden, C., Streets, D.G., Trautmann, N.M., 2007. Historical emissions of black and organic carbon aerosol from energy-related combustion, 1850–2000. Global Biogeochemical Cycles 21, GB2018. doi:10.1029/2006GB002840.

Chen, L.-W.A., Chow, J.C., Arnott, W.P., Moosmüller, H., Watson, J.G., 2004. Modeling reflectance and transmittance of quartz-fiber filter samples containing elemental carbon particles: implications for thermal/optical analysis. Journal of Aerosol Science 35, 765–780.

Chen, Y., Bond, T.C., 2010. Light absorption by organic carbon from wood combustion. Atmospheric Chemistry and Physics 10, 1773–1787.

Cheng, J.Y.W., Chan, C.K., Lau, A.P.S., 2011. Quantification of airborne elemental carbon by digital imaging. Aerosol Science and Technology 45, 581–586.

Chow, J.C., Watson, J.G., Crow, D., Lowenthal, D.H., Merrifield, T., 2001. Comparison of IMPROVE and NIOSH carbon measurements. Aerosol Science and Technology 34, 23–34.

Chow, J.C., Watson, J.G., Pritchett, L.C., Pierson, W.R., Frazier, C.A., Purcell, R.G., 1993. The DRI thermal/optical reflectance carbon analysis system: description, evaluation and applications in United States air quality studies. Atmospheric Environment 27A, 1185–1201.

Ezzati, M., Kamen, D.M., 2002. The health impact of exposure to indoor air pollution from solid fuels in developing countries: knowledge, gaps and data needs. Environmental Health Perspectives 110, 1057–1068.

Flanner, M., Zender, C.S., Hess, P., Mahowald, N., Painter, T., Ramanathan, V., Rasch, P., 2009. Springtime warming and reduced snow cover from carbonaceous particles. Atmospheric Chemistry and Physics 9, 2481–2497.

Hansen, A.D.A., Rosen, H., Novakov, T., 1984. The Aethalometer – an instrument for the real time measurement of optical absorption by aerosol particles. Science of the Total Environment 36, 191–196.

IPCC, 2007. Summary for policymakers. In: Solomon, S., Qin, D., Manning, M., Chen, Z., Marquis, M., Averyt, K.B., Tignor, M., Miller, H.L. (Eds.), Climate Change 2007: The Physical Science Basis. Contribution of Working Group I to the Fourth Assessment Report of the Intergovernmental Panel on Climate Change. Cambridge University Press, Cambridge, United Kingdom and New York, NY, USA.

Jacobson, M.Z., 2010. Short-term effects of controlling fossil-fuel soot, biofuel soot and gases, and methane on climate, Arctic ice, and air pollution health. Journal of Geophysical Research 115, D14209.

Kirchstetter, T.W., Novakov, T., Hobbs, P.V., 2004. Evidence that the spectral dependence of light absorption by aerosols is affected by organic carbon. Journal of Geophysical Research 109, D21208.

Moosmüller, H., Chakrabarty, R.K., Arnott, W.P., 2009. Aerosol light absorption and its measurement: a review. Journal of Quantitative Spectroscopy & Radiative Transfer 110, 846.

NIOSH, 1996. Elemental carbon (diesel particulate) method 5040. NIOSH Manual of Analytical Methods, fourth ed. National Institute for Occupational Safety and Health, Cincinnati, Ohio (1st Suppl.).

Pachauri, R.K., Sridharan, P.V. (Eds.), 1998. Looking Back to Think Ahead: GREEN India 2047. Tata Energy Research Institute, New Delhi, India.

Ramanathan, N., Ramana, M., Lukac, M., Siva, P., Ahmed, T., Kar, A., Rehman, I.H., Ramanathan, V., 2010. Cellphones as a Distributed Platform for Black Carbon Data Collection. American Geophysical Union. Fall meeting, 2010. Abstract #947311.

Ramanathan, V., Balakrishnan, K., 2007. Project Surya: reduction of air pollution and global warming by cooking with renewable sources. White paper, available at. http://www.projectsurya.org/storage/Surya-WhitePaper.pdf.

Ramanathan, V., Carmichael, G., 2008. Global and regional climate changes due to black carbon. Nature Geoscience 1, 221–227.

Ramanathan, V., Xu, Y., 2010. The Copenhagen Accord for limiting global warming: criteria, constraints, and available avenues. Proceedings of the National Academy of Sciences of the United States of America 107 (18), 8055–8062.

Schauer, J.J., Mader, B.T., Deminter, J.T., Heidemann, G., Bae, M.S., Seinfeld, J.H., Flagan, R.C., Cary, R.A., Smith, D., Huebert, B.J., BertramHowell, S., Kline, J.T., Quinn, P., Bates, T., Turpin, B., Lim, H.J., Yu, J.Z., Yang, H., Keywood, M.D., 2003. ACE-Asia inter-comparison of a thermal-optical method for the determination of particle-phase organic and elemental carbon. Environmental Science and Technology 37, 993–1001.

Schmid, O., Artaxo, P., Arnott, W.P., Chand, D., Gatti, L.V., Frank, G.P., Hoffer, A., Schnaiter, M., Andreae, M.O., 2006. Spectral light absorption by ambient aerosols influenced by biomass burning in the Amazon Basin. I: comparison and field calibration of absorption measurement techniques. Atmospheric Chemistry and Physics 6, 3443–3462.

Schwarz, J.P., Gao, R.S., Fahey, W., Thomson, D.S., Watts, L.A., Wilson, J.C., Reeves, J.M., Darbeheshti, M., Baumgardner, D.G., Kok, G.L., Chung, S.H., Schulz, M., Hendricks, J., Lauer, A., Karcher, B., Slowik, J.G., Rosenlof, K.H., Thompson, T.L., Langford, A.O., Loewenstein, M., Aikin, K.C., 2006. Single-particle measurements of midlatitude black carbon and light-scattering aerosols from the boundary layer to the lower stratosphere. Journal of Geophysical Research 111. doi:10.1029/2006JD007076.

Shindell, D., Faluvegi, G., 2009. Climate response to regional radiative forcing during the twentieth century. Nature Geoscience 2, 294–300.

Stephens, M., Turner, N., Sandberg, J., 2003. Particle identification by laser-induced incandescence in a solid-state laser cavity. Applied Optics 42, 3726–3736.

Venkataraman, C., Sagar, A.D., Habib, G., Lam, N., Smith, K.R., 2010. The Indian national initiative for advanced biomass cookstoves: the benefits of clean combustion. Energy for Sustainable Development 14, 63–72.